Surfaces and Interfaces 56 (2025) 105456

Contents lists available at ScienceDirect

Surfaces and Interfaces

journal homepage: www.sciencedirect.com/journal/surfaces-and-interfaces

CuO surface functionalized β-cyclodextrin grafted PMMA hybrid nanocomposite for advance oxidative mineralization of methyl orange

Imran Hasan [a,*], Akshara Bassi [b], Parvathalu Kalakonda [c]

[a] Department of Chemistry, College of Science, King Saud University, Riyadh 11451, KSA, Saudi Arabia
[b] Environmental Research Lab, Department of Chemistry, Chandigarh University, Mohali, Punjab, 140413, India
[c] Dept of Physics, Smart Nano Materials Research Laboratory, Government City PG College Autonomous, Osmania University, Hyderabad, Telangana, 50002, India

ARTICLE INFO

Keywords:
Nanocomposite
Methyl orange
Pmma
B-cyclodextrin
Photocatalytic degradation

ABSTRACT

The present study emphasizes the synthesis of copper (II) oxide (CuO) surface grafted with β-cyclodextrin (β–CD) copolymerized polymethylmethacrylate (PMMA) through in situ free radical oxidative polymerization reaction. The synthesized material CDMA@CuO nanocomposite (NC) material was thoroughly characterized using a range of instrumental techniques, including Scanning Electron Microscopy with Energy Dispersive X-ray (SEM-EDX), X-ray Diffraction (XRD), Transmission Electron Microscopy with Selected Area Electron Diffraction (TEM-SAED), Fourier Transform Infrared Spectroscopy (FTIR), Zeta potential measurement, X-ray Photoelectron Spectroscopy (XPS) and UV–vis spectroscopy. These analyses offered comprehensive insights into the composition, structure, optical, and surface properties of the synthesized material. The CDMA@CuO NC material was then assessed as a photocatalyst for the degradation of methyl orange (MO) dye under sunlight exposure. Notably, the material demonstrated outstanding photocatalytic activity, achieving a 99.37 % photocatalytic efficiency with 20 mg L^{-1} MO concentration at pH 4 under 90 min of UV light exposure. The trapping experiments confirmed the presence of hydroxyl radicals ($^{\bullet}OH$) as the primary reactive oxidant species responsible for MO photodegradation. The synthesized material exhibited efficient reusability for up to six consecutive cycles while maintaining its high photodegradation efficiency. These results emphasize the potential of the CDMA@CuO NC as a highly efficient and recyclable photocatalyst for the removal of organic contaminants, such as methyl orange from aqueous solutions.

1. Introduction

Organic dyes, recently introduced by the textile industry, are raising concerns due to their potential harm and difficulty in degradation [1]. Among various organic dyes, Methyl orange (MO), an anionic azo dye with the chemical formula ($C_{14}H_{14}N_3NaO_3S$) widely utilized in food, pharmaceutical, cosmetics, paper, and textile sectors for coloring purposes [2]. MO exhibits a persistent and complex structure, rendering it non-biodegradable and environmentally troublesome [2,3]. Its high stability and solubility in water contribute to its toxicity [4]. The negative impact of MO extends to mutagenicity and carcinogenicity, posing a threat to ecosystems through the presence of amines resulting from the reduction of azo group linkages [5,6]. Contamination of water bodies with MO hampers sunlight penetration, diminishing photosynthesis and adversely affecting aquatic life [7]. Moreover, MO and its derivatives have been linked to various health issues, including skin rashes, headaches, seizures, joint pain, nausea, and heart diseases [8,9]. The release of such persistent organic dye underscores the importance of addressing their environmental and health implications in various industries [10].

The most common methods for dye treatments include oxidation, coagulation, flocculation, ion exchange, adsorption, and photocatalytic [11–14]. Out of all these methods, the photocatalytic method gained more consideration with more advantages due to its low cost, eco-friendly, high chemical stability of the catalyst, non-toxic, and highly efficient method [15]. In the photocatalytic process, a semiconductors-based photocatalyst generates electron-hole pairs when exposed to light, leading to the formation of radicals such as superoxide and hydroxyl [16]. Under the influence of UV–vis radiations, these radicals then facilitate the breakdown of organic pollutants into non-toxic molecules [17,18].

Various metal oxide semiconductors, including ZnO, TiO_2, MnO_2,

* Corresponding author.
E-mail addresses: iabdulateef@ksu.edu.sa (I. Hasan), bassiakshara@gmail.com (A. Bassi), parvathalu.k@gmail.com (P. Kalakonda).

https://doi.org/10.1016/j.surfin.2024.105456
Received 10 September 2024; Received in revised form 3 November 2024; Accepted 15 November 2024
Available online 22 November 2024

CuO, Co_3O_4 etc., serve as photocatalysts due to their chemical, thermal, optical, and electrical properties [19]. Among these oxides, CuO, a p-type semiconductor with a band gap of 3.56 eV exhibits a monoclinic crystal structure [20]. Its widespread use in various applications such as solar cells, lithium batteries, storage media, cosmetics, pharmaceutics, and catalysis is attributed to its environmental compatibility and abundance [21,22]. The electrochemical and physicochemical properties of CuO NPs have been extensively studied for their role as catalysts, particularly as photocatalyst [23]. There are certain factors such as poor light absorption in visible light, photo corrosion and high rate of electron-hole pair recombination affect their photocatalytic activity [24]. To address this issue, researchers have applied certain methods such as a change in morphology, doping of heteroatom, formation of homo or heterojunction, change in synthesis method, and introduction of plasmonic metal atom (Ag, Au, etc.).

In the degradation of dyes, the fabrication of various inorganic-organic materials involves the incorporation of metal nanoparticles and natural biopolymers. Among various biopolymers, β-cyclodextrin (β-CD) is notable, comprising a cyclic oligosaccharide with seven-membered D-glucose monomers linked with α−1,4 glycosidic bonds [25,26]. This structure enhances water solubility and bioavailability of guest molecules through complexation, due to β-CD's spacious cavity [25]. The hydrophobic interior and hydrophilic exterior of β-CD, facilitated by its OH and R–OH group functional groups, make it valuable for complexation purposes. β-CD finds widespread application in the pharmaceutical and food industry, drug delivery, electromagnetic sensors, and the removal of pollutants from wastewater [27,28]. Polymers, being a cost-effective material, serve as an excellent immobilization matrix for photocatalysts. Poly methyl methacrylate (PMMA) is an optical lightweight transparent thermoplastic, lightweight, water-insoluble, and low-density [25]. PMMA exhibits properties such as scratch and water resistance, elastic modulus, UV absorption, and thermal stability, making it suitable for applications in photocatalysis and biomedical applications. When PMMA is combined with metal oxides, it forms a composite with enhanced electro-thermal and mechanical stability [29,30]. Due to its hydrophobic nature, PMMA interacts with dye molecules, facilitating the removal of dyes from the water [31]. The optical absorption range of CuO is expanded into the visible region by incorporating it with β–cyclodextrin (β-CD) and PMMA, which helps overcome electron-hole recombination during the photocatalytic process.

This work presents a novel approach to advanced oxidative mineralization of methyl orange (MO) dye by synthesizing a CuO surface-functionalized, β-cyclodextrin (β-CD) grafted PMMA hybrid nanocomposite. This innovative approach integrates the advantages of each component CuO nanoparticles, β-cyclodextrin, and PMMA to create a multifunctional composite with unique properties that address current limitations in the degradation of organic pollutants. By using β-cyclodextrin a naturally derived, biodegradable compound the synthesis approach aligns with green chemistry principles. The functional design reduces the need for harsh chemical additives and supports an environmentally benign pathway for MO degradation. This unique combination enables efficient oxidative degradation of MO, offering an environmentally friendly and highly efficient strategy for wastewater treatment applications that target persistent organic pollutants.

2. Materials and methods

2.1. Chemicals and reagents

Copper nitrate [Cu $(NO_3)_2$•$5H_2O$] hemi pentahydrate 98 % was purchased from Merck, India. Methyl methacrylate (MMA) (99 %) was purchased from Loba Chemie India. β-cyclodextrin (CD), potassium persulfate, and N, N-methylene bis-acrylamide (MBA) were purchased from Sigma Aldrich, India. Sodium hydroxide (NaOH) was purchased from Merck, India. Methyl Orange was purchased from Otto Chemical Pvt. Ltd, India. The experiment involved the precise measurement of salts and reagents according to stoichiometry, with deionized water utilized throughout the procedures. To prepare the standard solution of methyl orange at a concentration of 1000 mgL^{-1}, an accurate quantity of the dye was dissolved in 100 mL of deionized water.

2.2. Synthesis of CDMA@CuO nanocomposite

2.2.1. Synthesis of copper oxide nanoparticles

The synthesis of copper oxide nanoparticles was conducted via the sol-gel method. Initially, in a round bottom flask, 2 M of copper nitrate was dissolved in 100 mL of solution and stirred for 1 h at 40 °C. Subsequently, 20 mL of 1 M NaOH solution was added dropwise with constant stirring at 1200 rpm for 3 h The resulting nanoparticles were then washed with deionized water to eliminate any unreacted species. Finally, the nanoparticles were dried in a vacuum oven at 40 °C for 2 h.

2.2.2. Synthesis CDMA@CuO nanocomposite

The nanocomposite material was synthesized using an in situ chemical co-precipitation method associated in conjunction with the solvent casting method. The detailed procedure is as follows; A solution containing 1 M of CuO NPs solution and 2 g of β-cyclodextrin powder was prepared, and the mixture was subjected to constant stirring at 1200 rpm for 3 h Subsequently, 20 mL of a 3 % KPS solution was added dropwise to the β-CD@CuO solution, along with 0.75 g N, N- methylene bis-acrylamide, and the mixture was stirred for an additional 2 h To this solution, 10 mL of methyl methacrylate monomer was added, and the reaction was allowed to proceed for 12 h at 60 °C with continuous stirring at 1200 rpm. The nanocomposite was obtained by pouring the resulting white suspension into an excess amount of methyl alcohol. The product was washed with methyl alcohol and then with deionized water to remove any unreacted monomer, followed by drying in a vacuum oven at 60 °C for 4 h

2.3. Analytical instrument for characterization of CDMA@CuO NC

The crystal structure, morphology, and optical change in CDMA@-CuO NC were thoroughly examined through different analytical techniques. The bond formation and functional group were analysed using a Fourier transform infrared (FTIR) spectrophotometer, specifically the Perkin Elmer Spectrum 2 ATR model, covering a frequency range of 400–4000 cm^{-1}. The morphology of the nanocomposite was investigated by using a Scanning electron microscope (SEM), specifically the GSM 6510LV, JOEL, in conjunction with energy diffraction X-ray (EDX) to determine the elemental composition. The particle size and its distribution in the polymer matrix, and chemical homogeneity were assessed using a Transmission electron microscope (TEM), employing the JEM 2100, Japan. The oxidation state and chemical composition of an individual constituent in the material were analyzed using X-ray photoelectron (XPS) spectroscopy with the PHI 5000 Versa Probe II, FEI Inc. The dynamic size of the synthesized material in solvent media was determined using Zeta sizer advance by Malvern Panalytical. The optical properties, including the energy band gap of the material and the concentration of MO dye, were examined using a double-beam UV–vis spectrophotometer, specifically the Shimadzu UV-1900.

2.4. Photocatalytic experiment

Before conducting the photocatalytic degradation experiment, a selectivity test was carried out for various dyes, drugs, and phenolic compounds using the synthesized material. Based on the results, it was determined that MO dye was selected for photocatalytic degradation. The photocatalytic degradation of MO dye was performed in the presence of a UV light source i.e., halogen lamp (50 W) using a 25 mL of aliquot with varying concentrations of MO (10–40 mgL^{-1}) solution. It was observed that the dye degradation increased in the presence of a halogen lamp and catalyst. Subsequently, different parameters such as time (10–90 min), pH (1–10), and catalyst dose of 25 mg were applied

under the influence of the halogen lamp. In the photocatalytic reactor, the MO dye effluents were analysed using a UV–VIS spectrophotometer at the maximum absorption wavelength of λ_{max}= 467 nm. The percentage degradation was further calculated by using the formula given as

$$\text{Photocatalyticefficiency}(\%) = \frac{C_0 - C_t}{C_0} \times 100 \quad (1)$$

where C_o and C_t are the initial and final concentrations of MO dye after the photocatalysis. The obtained data was processed using MS Excel software and Origin 9.1.

3. Results and discussion

3.1. Characterisation of CDMA@CuO NC

Fig. 1 illustrates the FTIR spectra of the CDMA@CuO NC material along with its constituent molecules. Fig. 1(a) displays the FTIR spectrum of CuO NPs with absorption peaks at 3569 cm^{-1} (-OH stretching), 3388 cm^{-1}, 1098 cm^{-1} (C—O bending), 869 cm^{-1} (-H_2O rocking), 775 cm^{-1} (Cu $(OH)_2$ stretching) and 601 cm^{-1} (Cu-O stretching) [32]. In Fig. 1(b), the FTIR spectrum of β-CD exhibits absorption peaks at 3301 cm^{-1} (-OH vibrations), 2890 cm^{-1} (C—O-C stretching), 1643 cm^{-1} and 1019 cm^{-1} (-CH_2 asymmetric stretching) [33]. In Fig. 1(c), the FTIR spectrum of PMMA reveals the absorption peaks at 3451 cm^{-1} (–OH vibrations), 2954 cm^{-1} (–CH_3 and =CH_2 vibrations), 1737 cm^{-1} (C = O group), 1454 cm^{-1} (C–O group), 1264 cm^{-1}, 1170 cm^{-1} (C–O–C group), 979 cm^{-1} (–CH═CH), 846 cm^{-1} (C–H and –CH_3 vibrations) and 751 cm^{-1} (C—H bending) [34]. Fig. 1 (d-f), the FTIR spectrum of CDMA@CuO NC demonstrates absorption peaks at 3341 cm^{-1} (–OH stretching), 2985 cm^{-1} (–CH_3 and =CH_2 vibrations), 1722 cm^{-1} (C = O group), 1454 cm^{-1} (C–O group), 1145 cm^{-1} (C–O–C group), 972 cm^{-1} (–CH═CH), 751 cm^{-1} (Cu $(OH)_2$ stretching) and 601 cm^{-1} (Cu–O stretching) [35]. As the concentration of copper oxide increases in CDMA@CuO-1 %, CDMA@CuO-2 %, and CDMA@CuO-3 %, the peaks become sharper, suggesting an enhancement in the degree of immobilization of CuO by β-CD-PMMA copolymer chain.

Fig. 2 illustrates the XRD spectra of (a) CuO, (b) PMMA (c) CDMA@CuO-1 %, (d) CDMA@CuO-2 %, and (e) CDMA@CuO-3 % NC providing insights into the lattice and crystalline structure of the nanocomposite concerning increase in nanofiller concentration. In the XRD spectra, the black line representing CuO NPs reveals 2θ values of 13.9°, 16.7°, 22.9°, 28.1°, 35.8° and 52.7°, corresponding to miller indices of (021), (110), (002), (111), (220) and (113) respectively [35]. The red line representing PMMA displays the 2θ values of 13.4°, 27.3° and 30.8°, corresponding to miller indices of (111), (112) and (211) respectively [36]. The blue line representing CDMA@CuO–1 % NC exhibits 2θ values of 21.3°, 24.2°, 30.0°, 37.9° and 71.1°, corresponding to miller indices of (100), (101), (110), (102) and (104) respectively. Upon comparing the XRD spectra, it is inferred that the synthesized NC material consists of CuO NPs immobilized within the β-CD-PMMA polymer matrix. Further details regarding the % crystallinity and crystallite size can be computed using the given equation. To calculate the crystallite size, the equation Scherrer formula is employed [37]-

$$D = \frac{0.9 \times \lambda}{\beta \times \cos\theta} \quad (2)$$

$$\text{Crystallinity}(\%) = \frac{\text{Areaunderthecrystallinepeak}}{\text{Totalarea}} \times 100 \quad (3)$$

Where λ stands for the frequency of radiation, θ stands for the diffraction angle, β stands for half the width of intense peaks and D is crystallite size (nm). The crystallite size of CuO NPs, PMMA, CDMA@CuO-1 %, CDMA@CuO-2 %, and CDMA@CuO-3 % NC were determined. Using Eq. (2), yielding values of 7.4 nm, 15.6 nm, 20.7 nm, and 29.1 nm respectively. According to Eq. (3), the crystallinity percentage were found to be 72.6 % for CuO NPs, 19.84 % for PMMA (80.16 % amorphous), 29.21 % for CDMA@CuO-1 % (70.79 % amorphous), 32.12 % for CDMA@CuO-2 % (67.88 % amorphous) and 45.34 % for CDMA@CuO-3 % NC (54.66 % amorphous). The amorphous nature of CDMA@CuO NC can be attributed to the presence of the β-CD-PMMA polymer matrix

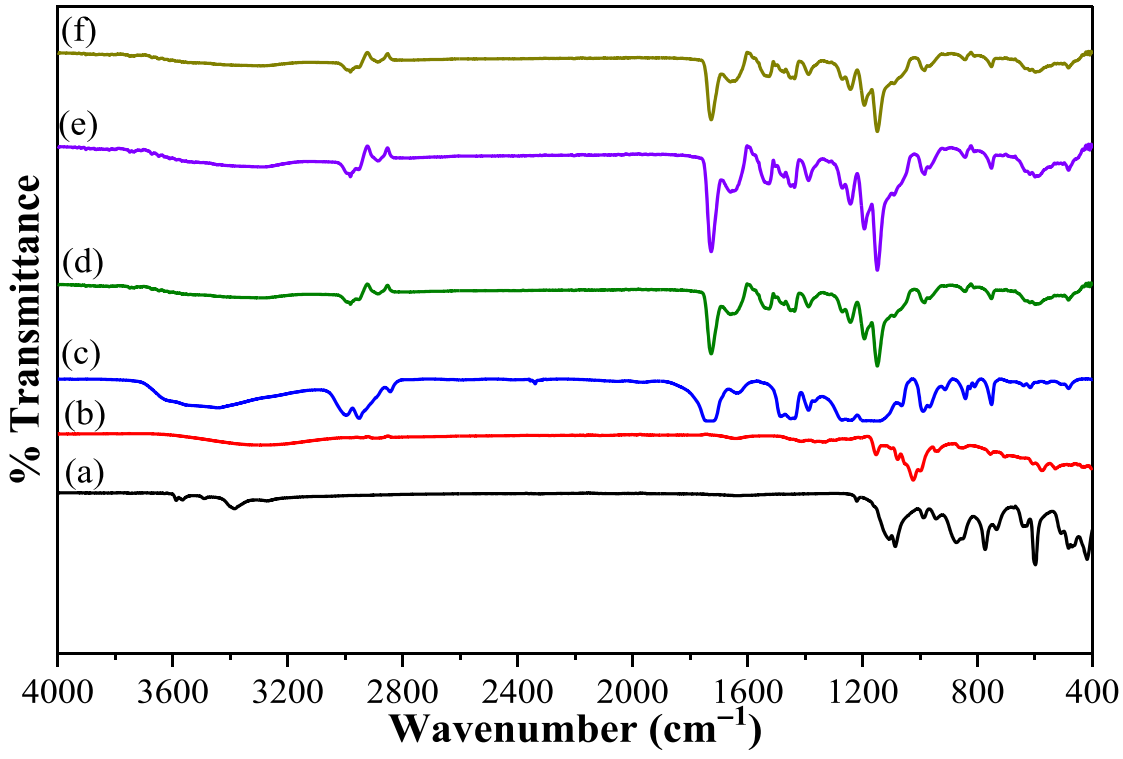

Fig. 1. FTIR of (a) CuO, (b) β-CD, (c) PMMA, and (d) CDMA@CuO-1 % (e) CDMA@CuO-2 % and (f) CDMA@CuO-3 % NC.

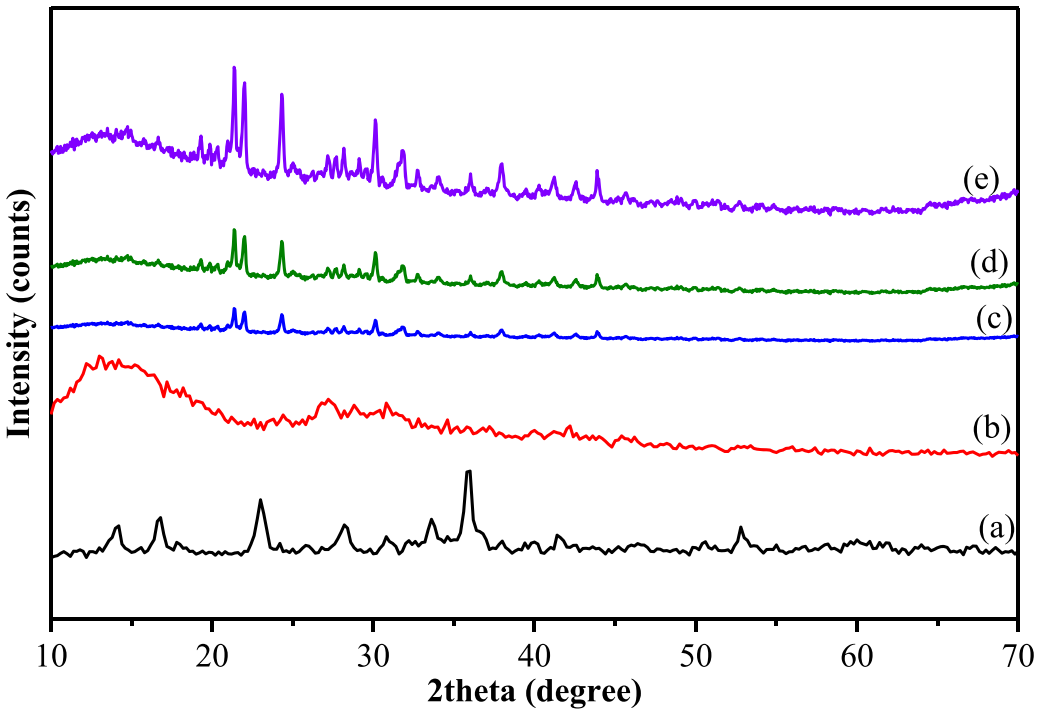

Fig. 2. XRD spectra of (a) CuO, (b) PMMA, (c) CDMA@CuO-1 %, (d) CDMA@CuO-2 %, and (e) CDMA@CuO-3 % NC.

effectively encapsulating the CuO NPs. It can be observed that as the concentration of CuO increases in the copolymer matrix of β-CD-PMMA, the amorphous nature keeps on decreasing due to the crystalline effect of CuO NPs.

The surface morphology of CuO NPs, PMMA, is presented in Fig. 3 (a, b). The SEM image of CDMA@CuO-1 %, CDMA@CuO-2 %, and CDMA@CuO-3 % NC, along with their elemental analysis, is presented in Fig. 3 (c-e). In Fig. 3(a), the SEM image of CuO NPs reveals spherical shapes distributed throughout the space-adjusted framework. Fig. 3(b) displays the SEM image of PMMA, showcasing a continuous matrix with a fracture surface and small nodules exhibiting low crystallinity. Fig. 3 (c-e) exhibits the SEM image of CDMA@CuO-1 %, CDMA@CuO-2 %, and CDMA@CuO-3 % NC a combination of spherical and flaky structure, indicating that CuO NPs are encapsulated by the layer of β-CD-PMMA polymer matrix. Fig. 3 (f-h) presents the energy disperive X-ray (EDX) spectra, analyzing the elemntal composition of the synthesized material within energy range of 1–20 keV. The atomic percentage of elements was found to be in CDMA@CuO-1 % was C (64.59 %), O (32.23 %) and Cu (3.18 %) in CDMA@CuO-2 % C (59.01 %), O (34.77 %) and Cu (6.22 %) was and CDMA@CuO-3 % was C (53.78 %), O (37.78 %) and Cu (8.45 %). These results affirm the purity of synthesized material. Fig. 3 (i) displays the compositional SEM image illustrating elemental mapping for CDMA@CuO-3 %, where the distribution of all elements i.e., C (K) as red dots, O(K) as green dots and Cu(K) as blue dots appears uniform throughout the spatial range. This observation is further substantiated by Figure S1 (a,b) explaining one material dense i.e., Cu in the case of CDMA@CuO-3 %.

The TEM image provides insights into the particle size and its distribution in the polymer matrix, and the chemical homogeneity. Fig. 4 (a-c) shows the TEM image of CDMA@CuO-1 %, CDMA@CuO-2 %, and CDMA@CuO-3 % are spherical structure and finely distributed CuO NPs in the β-CD-PMMA matrix are evident. Fig. 4(d) represents the Gaussian distribution profile for particle size showcasing an average particle size are 12 nm, 18 nm, and 25 nm, respectively, consistent with the results obtained from XRD analysis. It can be seen that as the concentration of Cu increases, the particle size keeps on increasing due to agglomeration.

X-ray photoelectron (XPS) spectra were utilized to analyze the chemical composition and oxidation state of the individual constituents in the CDMA@Cu-3 % NC material. Fig. 5(a) illustrates the survey scan of CDMA@CuO-3 % NC, revealing explains the presence of oxygen, carbon, nitrogen, and copper. Fig. 5(b) displays the binding energy with triplet peaks at 283 eV, 284.4 eV, and 286.8 eV, corresponding to C−C/C–H, C–O, and C = O respectively, in NC material attached to PMMA and BCD biopolymer chain [38]. In Fig. 5(c), the binding energy exhibits triplet peak value at 530.5 eV, 529.1 eV, and 532.1 eV corresponding to C—O-H/C–O–C, C = O, and C—O-C respectively [39]. Fig. 5(d) shows the binding energy with a triplet peak value at 398.2 eV, 397.8 eV, and 399.3 eV corresponding to pyrrolic, pyridinic, and graphitic nitrogen bonding respectively [40]. Fig. 5(e) illustrates the binding energy peaks of Cu2p indexed to 940 eV, 937.4 eV, and 935.4 eV corresponding to Cu $2p_{1/2}$, Cu $2p_{3/2}$, confirming the existence of CuO with +2 oxidation state [41]. The detailed XPS analysis provides insights into the chemical composition and bonding configuration of the CDMA@CuO NC material.

Zeta potential analysis was employed to determine the point of zero charge, elucidating the pH-dependent adsorption behavior of MO using synthesized NC material. A solution consisting of 25 mL of 0.1 KCl was prepared, and a particle suspension was achieved by adding 20 mg of NC material under sonication across a pH range from 1 to 10. Zeta potential values were observed at one-unit intervals within this pH range. The results are given in Figure S2, indicating a decrease in zeta potential from 350 mV at pH 1 to 72 mV at pH 10, revealing a zeta potential of approximately zero mV at pH 5.2. This particular pH marks the isoelectric point (IFP) or point of zero charge (PZC) on the catalyst's surface and corresponding pH values are termed as pH_{iep} or pH_{pzc}.

The band gap value and optical properties of pristine CuO and CDMA@CuO NC were determined using UV–Vis spectroscopy within the wavelength range of 200–500 nm. Fig. 6(a) represents the UV–vis absorption profile pristine CuO, CDMA@CuO-1 %, CDMA@CuO-2 %, and CDMA@CuO-3 %. The absorption maxima for pristine CuO were observed at λ_{max}= 270 nm which suggests the n-π^* electronic transitions. Further immobilization of the CuO surface with β-CD-PMMA copolymer chain with increasing CuO concentration results in a decrease in absorption intensity suggesting an increase in particle size of CuO NPs in

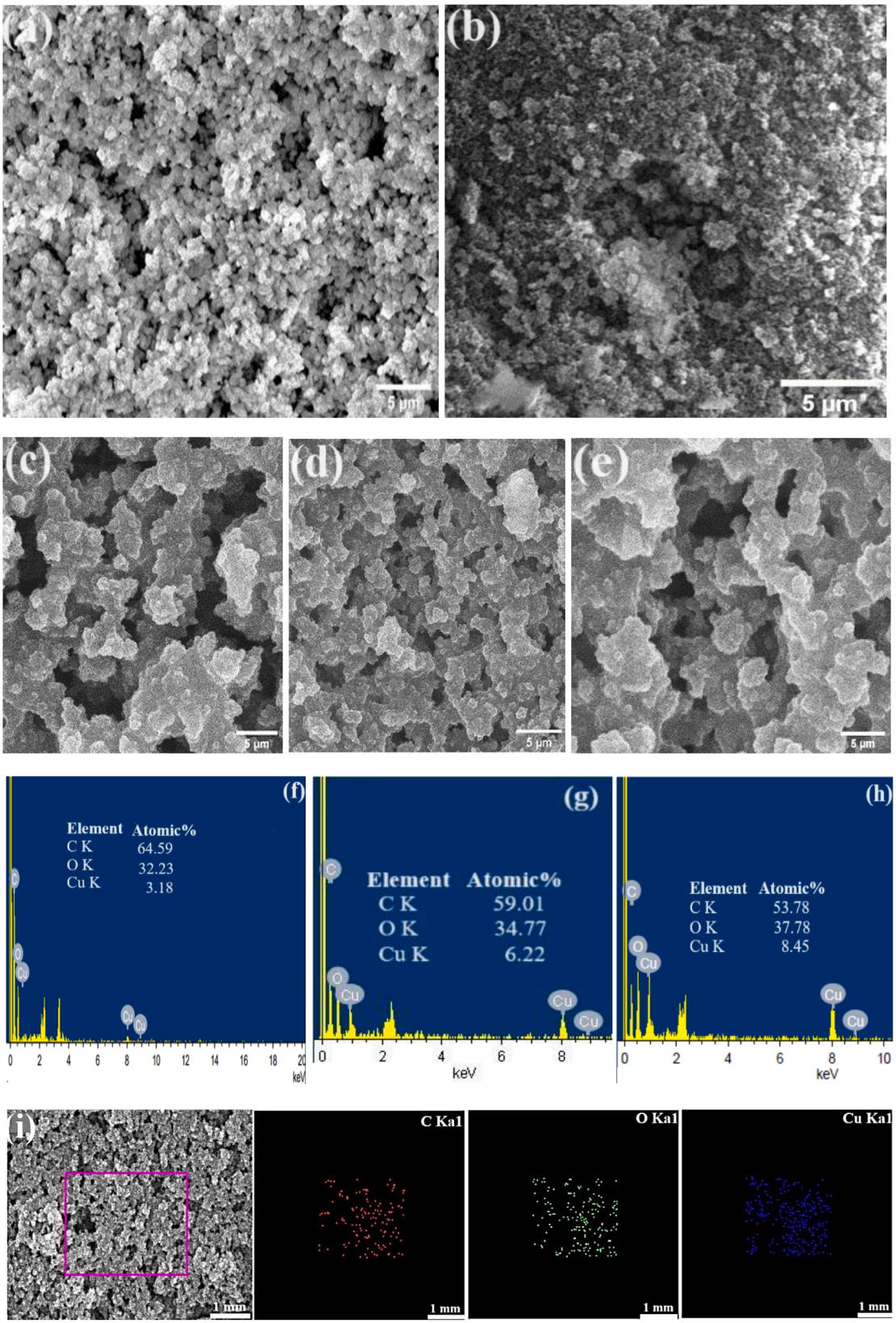

Fig. 3. (a) SEM image of CuO NPs, (b) SEM image of PMMA (c, f) SEM-EDX image of CDMA@CuO-1 %, (d,g) SEM-EDX image of CDMA@CuO-2 %, (e,h) SEM-EDX image of CDMA@CuO-3 % NC, (i) compositional SEM image of CDMA@CuO-3 % NC showing elemental distribution by red, green and blue dots, elemental mapping for C K, O K, and Cu K.

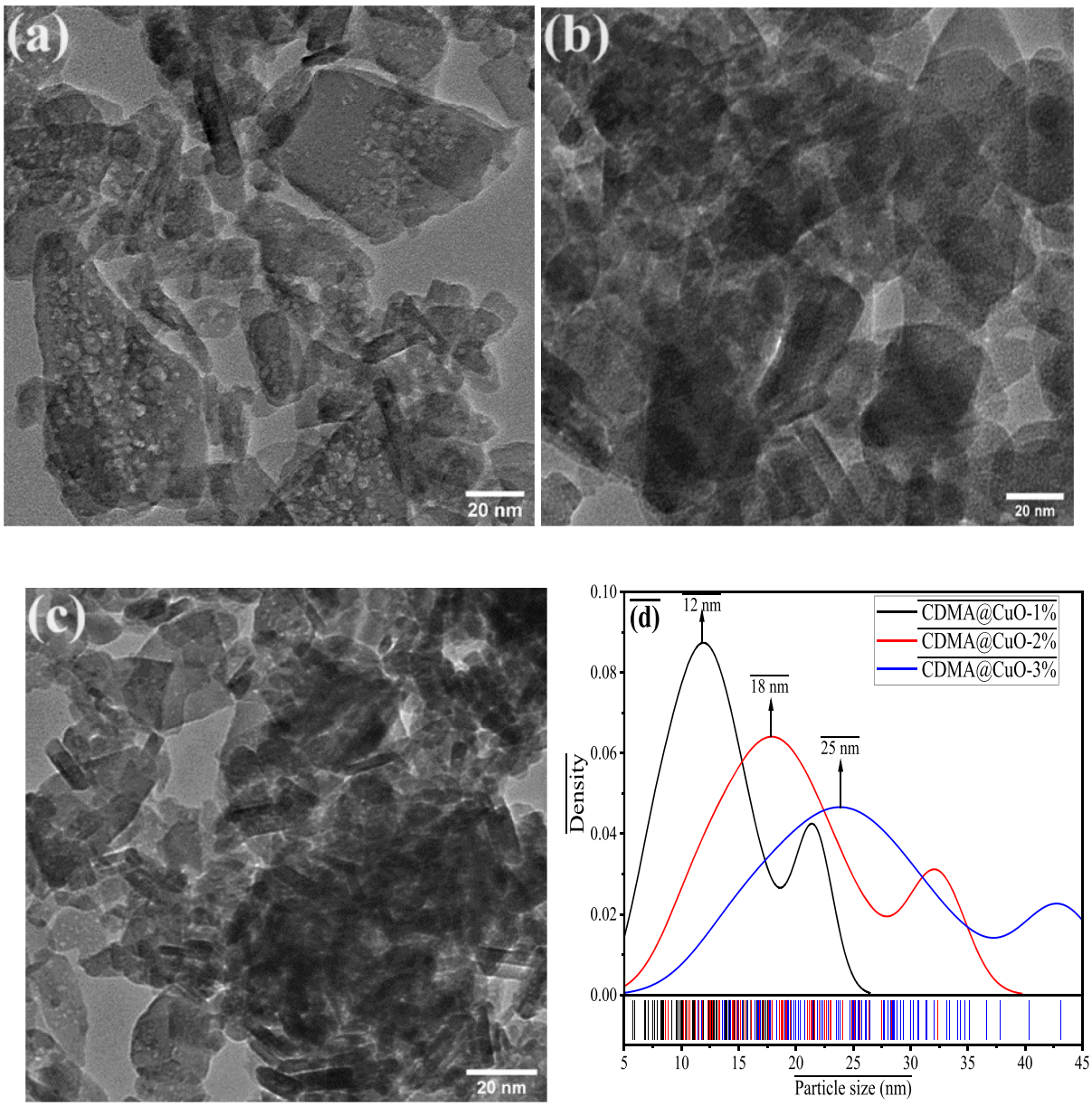

Fig. 4. TEM image of (a) CDMA@CuO-1 %, (b) CDMA@CuO-2 %, (c) CDMA@CuO-3 % NC, and (d) gaussian distribution profile for particle size.

association with successful immobilization of the surface. The direct and indirect band gap value of CDMA@CuO NC was calculated by Tauc's plot and the equation is given below [42];

$$\alpha hv = A(hv - E_g)^n \quad (4)$$

Here, v is the frequency, α is the absorption coefficient, h is the planks constant, A is constant, and n is the transition constant (n where 2 for the direct band and n= ½ for the indirect band). Fig. 6(b), the inserted graph represents Tauc's plot for the synthesized material, illustrating the direct band gap value. This graph is plotted between $(\alpha hv)^2$ and E_g (eV), with the exclusion of the direct band gap value of CDMA@CuO NC, which is determined to be 3.79 eV, 3.18 eV, 2.73 eV and 2.41 eV for pristine CuO NPs, CDMA@CuO-1 %, CDMA@CuO-2 % and CDMA@CuO-3 %. The reduction is attributed to quantum confinement effects, which stabilize the CuO NPs by βCD-PMMA matrix [39]. The values of bandgap suggest that CDMA@CuO-3 % having minimum bandgap may exhibit higher photocatalytic activity as compared to other variable materials.

The thermal stability of PMMA and the synthesised materials, namely CDMA@CuO-1 %, CDMA@CuO-2 % and CDMA@CuO-3 % was investigated by using TGA analysis. TGA is a technique that measures changes in weight loss of a material as a function of temperature, providing insights into its thermal degradation behaviour, and the results are given in Figure S3. In the TGA profiles, PMMA exhibited an initial weight loss at 176 °C, corresponding to approximately 5 % of its weight loss, which was attributed to the evaporation of water content present within the material. The subsequent weight loss of about 2.6 % at 365 °C suggests the degradation of PMMA polymer chains, leading to the release of volatile compounds. For the synthesized materials, CDMA@CuO-1 %, CDMA@CuO-2 %, and CDMA@CuO-3 %, the initial degradation temperatures and weight losses varied. CDMA@CuO-1 % started to degrade at a higher temperature 272 °C compared to PMMA, indicating improved thermal stability. This could be attributed to the incorporation of CuO into the CDMA structure, which might enhance the material's resistance to thermal degradation. Similarly, CDMA@CuO-2 % and CDMA@CuO-3 % also exhibited higher initial degradation temperatures of 266 °C and 274 °C respectively compared to PMMA, with corresponding weight losses of 9.5 % and 15.4 %. The presence of

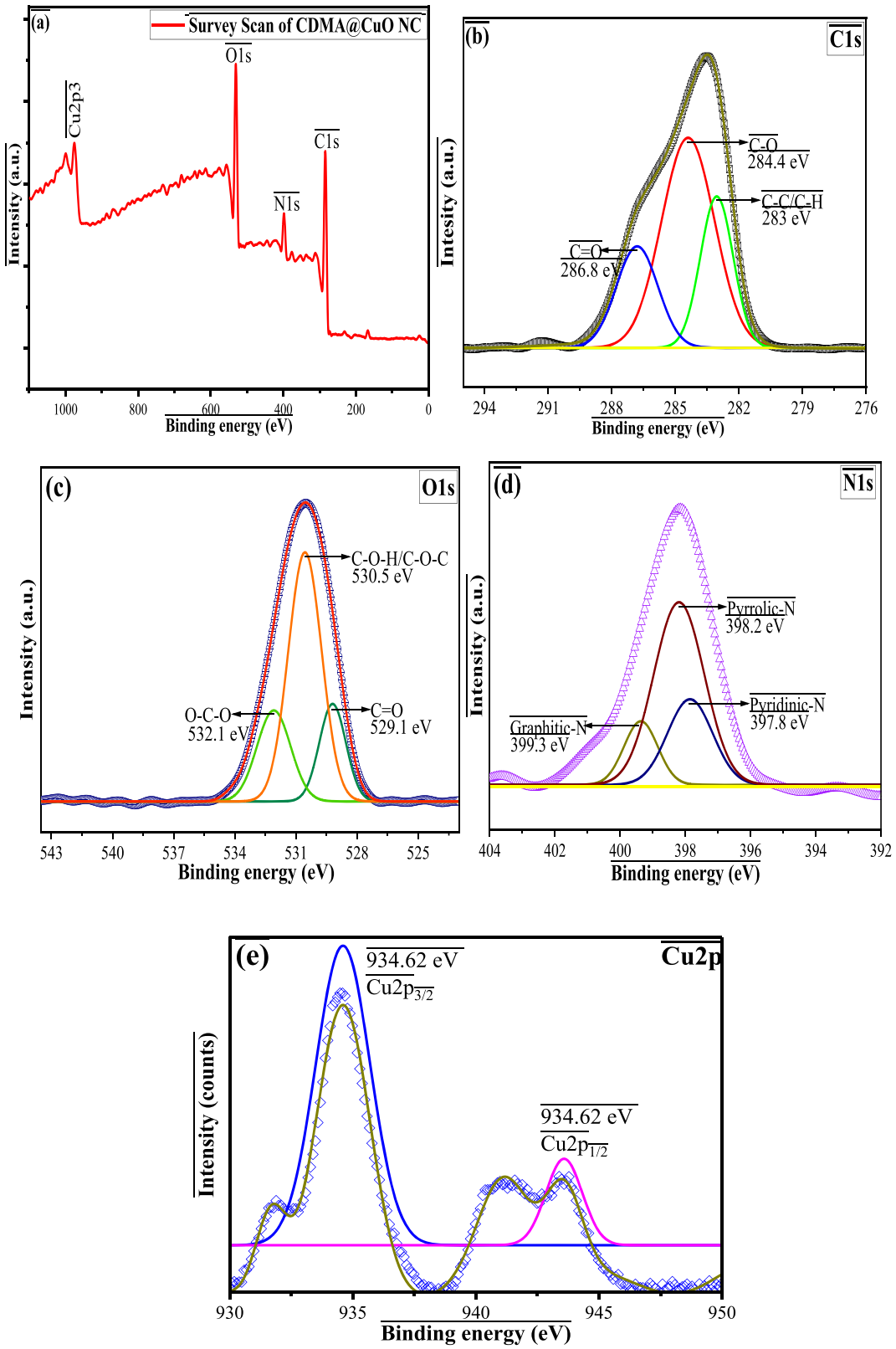

Fig. 5. XPS spectra of (a) CDMA@CuO-3 % NC survey, (b) C 1 s, (c) O 1 s, (d) N 1 s, and (e) Cu 2p3.

copper in these materials likely contributed to their enhanced thermal stability by facilitating strong intermolecular interactions or hindering the mobility of polymer chains. Furthermore, the successive weight losses observed at higher temperatures around 450–460 °C for all the synthesized materials can be attributed to the presence of copper [43].

The photoluminescence (PL) spectra of CuO NPs and CDMA@CuO-1 %, CDMA@CuO-2 %, and CDMA@CuO-3 % NC were observed and results are given in Fig. 7(a). PL spectra can provide insights into electron-hole recombination mechanisms and defect states within the material. [44] Pristine CuO NPs exhibit strong PL peaks due to efficient

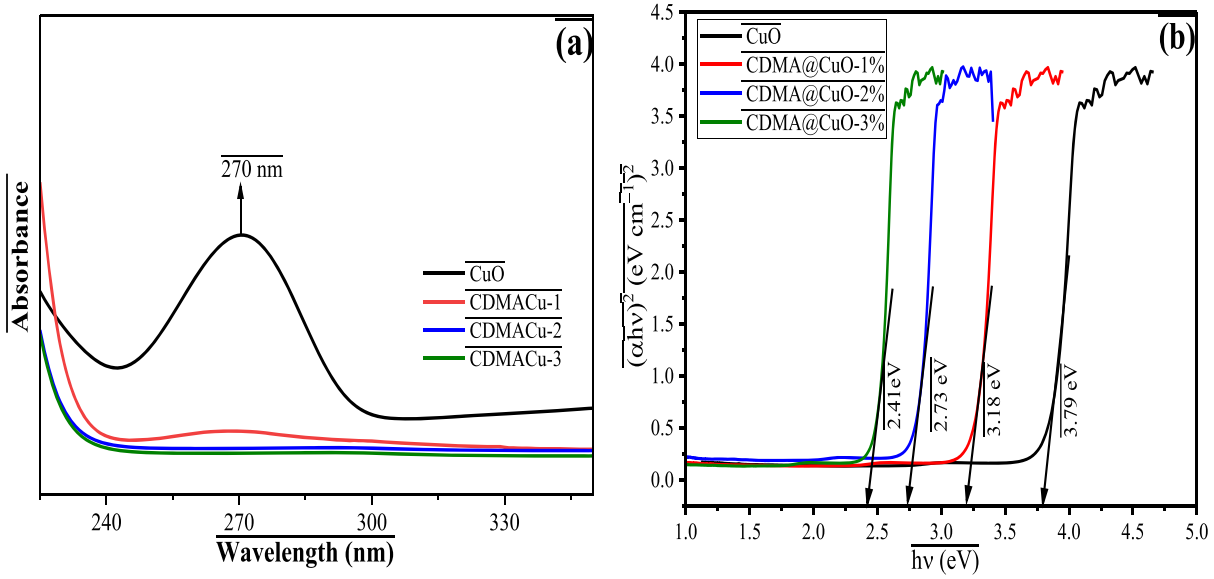

Fig. 6. (a) UV–Vis absorption spectra and **(b)** corresponding Tauc's plot for pristine CuO NPs, CDMA@CuO-1 %, CDMA@CuO-2 % and CDMA@CuO-3 % for calculating the band gap energy.

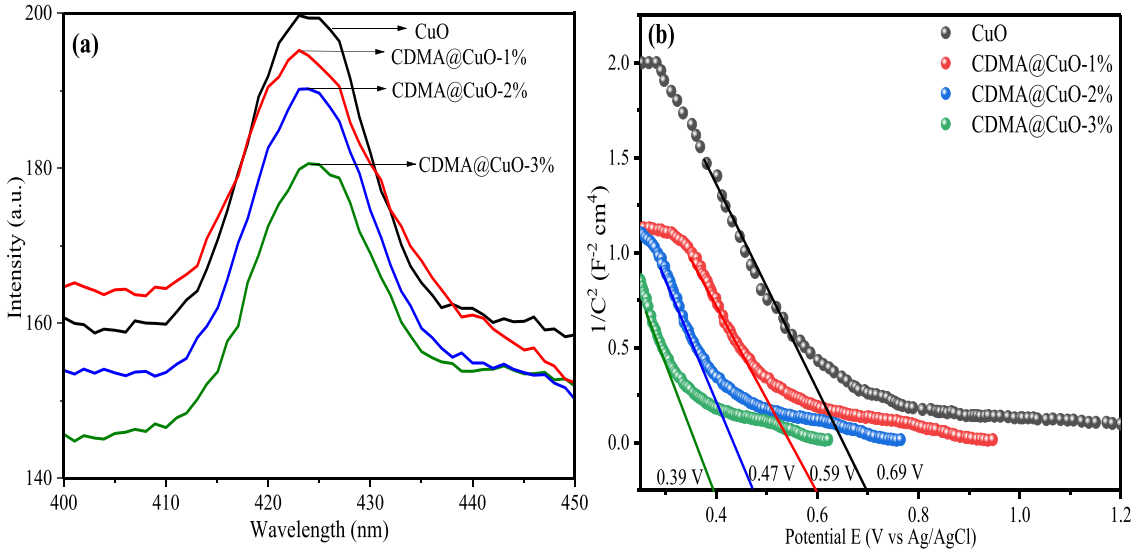

Fig. 7. (a) photoluminescence and (b) Mott-Schottky (M-S) spectra for CuO, CDMA@CuO-1 %, CDMA@CuO-2 % and CDMA@CuO-3 %.

electron-hole recombination. In CDMA@CuO-1 %, the PL intensity generally decreases, indicating a reduction in electron-hole recombination. This is likely due to the introduction of CDMA polymer blend, which can act as a charge carrier trap or as an electron acceptor. The CDMA molecules interact with CuO's electronic structure, effectively separating the electron-hole pairs and reducing their recombination rate. [45] With a further increase in CuO concentration to 2 %, the PL intensity decreased even more, demonstrating a more pronounced reduction in electron-hole recombination. At 3 % CuO concentration, the PL spectrum again displayed a further decrease in intensity. At this level, a balance is reached where the availability of electron traps or charge-separating sites maximizes the suppression of electron-hole recombination without overloading the system with excessive increase in concentration, which could introduce defects or cause agglomeration. Optimal charge separation at this concentration may yield the best performance in terms of energy conversion efficiency, making CDMA@CuO-3 % a potentially ideal composition for photocatalytic application.

The Mott-Schottky (M-S) analysis was conducted to investigate the electronic properties and interfacial synergy between CuO and the CDMA polymer blend in the synthesized nanocomposite materials CDMA@CuO-1 %, CDMA@CuO-2 %, and CDMA@CuO-3 % NC. The M-S curves of the CDMA@CuO nanocomposites given in Fig. 7(b) revealed an n-type semiconducting behaviour, consistent with the presence of CuO as the primary semiconductor material. [46] The calculated flat band potentials from the M-S curves shifted slightly with increased CuO concentration, CDMA@CuO-1 % (0.59 V), CDMA@CuO-2 % (0.47 V) and CDMA@CuO-3 % NC (0.39 V) indicating a higher carrier density than and suggesting that the CDMA polymer modifies the electronic environment around CuO. This shift could be attributed to changes in the surface states and band alignment between CuO and CDMA, which enhances the interfacial electron transfer dynamics. [47] The M-S findings therefore confirm that the CDMA polymer not only physically stabilizes CuO but also actively contributes to tuning the electronic properties of the composite material, likely due to the formation of an effective electronic network within the matrix.

The Brunauer–Emmett–Teller (BET) model is one of the most effective quantitative methods for calculating surface area. Here, we used N_2 gas adsorption and BET surface area analysis to investigate the pore size distribution and surface area of CuO nanoparticles (NPs) and CDMA@CuO-3 % NC. Both CuO NPs and synthesized hybrid material, exhibit a type IV isotherm with an adsorption-desorption curve shown in Figure S4. This type IV isotherm, observed through the hysteresis loop within the relative pressure range (P/P_o) of 0.8 to 0.9, confirms the mesoporous nature of the synthesized NPs. [48] A hysteresis loop is a distinguishing feature of type IV isotherms, typically associated with mesoporous materials. The surface areas for both CuO NPs and CDMA@CuO-3 % NC, measured using the standard multi-point BET method, were 18.23 m^2/g and 29.38 m^2/g, as shown in Figure S4. This increase in surface area can be attributed to the incorporation of CDMA, which likely contributes to a more dispersed and expanded structure, facilitating the availability of more active sites on the nanocomposite's surface and synergistically enhances the adsorption and photocatalytic activity of the material. [49] Pore size distribution, analysed using the Barrett-Joyner-Halenda (BJH) desorption method, revealed pore sizes of 3.69 nm and 8.24 nm. The increased pore size in the nanocomposite suggests that the incorporation of CDMA alters the porosity of CuO, creating larger mesopores that can facilitate molecular diffusion and transport. Together, the higher surface area and larger pore size of CDMA@CuO-3 % NC suggest an enhanced structural and functional design over CuO NPs. These characteristics may lead to improved catalytic efficiency and stability, making CDMA@CuO-3 % NC a promising candidate for applications requiring high surface activity and efficient molecular transport.

3.2. Photocatalytic experiment

The experiments were designed to examine the removal of dyes in the absence of a catalyst under light (photolysis), in the presence of a catalyst (adsorption), and in the presence of a catalyst under UV, Visible, and sunlight (photocatalysis), with the UV–VIS curve depicted in Fig. 8 (a). The experiments were performed by taking 50 mg L^{-1} MO dye with 20 mg catalyst under photocatalytic reactor for an irradiation time of 120 min. All three variables of the catalyst i.e., CDMA@CuO-1 %, CDMA@CuO-2 %, and CDMA@CuO-3 % were tested for the photocatalytic degradation of MO dye under various illumination conditions. It can be seen from Fig. 8(a) that in the presence of CDMA@CuO-3 %, MO dye exhibited minimum absorption maxima under UV light illumination. This indicates that CDMA@Cu-3 % is more effective at catalyzing the degradation reaction compared to the other catalytic variables under UV light irradiation.

Fig. 8(b) shows the effect of irradiation time on the degradation of MO by using CDMA@CuO-3 % in the aqueous solution was observed at different irradiation times. Fig. 8(b) shows the UV–VIS curve for the MO at 10–90 mins for 20 mg of catalyst dose and 20 mgL^{-1} of MO initial concentration. It was found that as the irradiation time increases, more time is available for the photocatalytic reaction to occur. Dye molecules have a greater opportunity to come into contact with the catalytic surface and undergo degradation because more photons are available to the activate the photocatalyst. Each photon absorbed by the catalyst generates electron-hole paors, which participate in the degradtion of dye molecules. This prolonged exposure to the catalyst allows for more dye molecules to be degraded, resulting in higher overall efficiency. Therefore, the rate of MO degradation is achieved at 90 mins of irradiation tiume.

Fig. 8(c) effect of pH of MO on the degradation of MO by using CDMA@CuO-3 % NC in the aqueous solution wasobserved at different pH. Fig. 8(c) shows the %degradation for the MO 1–10 pH range with respect to irradiation time at 90 mins for 20 mg of catalyst dose for 20 mgL^{-1} of MO initial concentration. The results obtained exhibited towards MO, yielding degradation rate of 57.95 % for pH 1, 73.97 % for pH 2, 94.37 % for pH 3, 98.77 % for pH 4, 96.51 % for pH 5, 93.02 for pH 6, 85.06 % for pH 7, 76.39 % for pH 8, 72.39 % for pH 9 and 63.51 % for pH 10. It was found that at different pH levels, the surface charge on the catalyst may vary due to chnages in the protobation and deprotonation of the surface functional groups. At pH 4, the surface charge of the catalyst and the dye molecules may be exhibit the strongest electrostatic interactions, facilitating the efficient adsorption of dye onto the catalyst surface. The concentration of hydroxyl ions ($^{\bullet}OH$) and hydrogen ions (H^{+}) promotes the generation of reactive oxygen species (ROS) on the catalyst surface which play a crucial role in oxidising the dyes molecules and promoting their degradation. At pH 4, the catalyst may exhibit the highest activity promoting the degradtion of the molecules throught efficient generation and utilizing of ROS.

Fig. 8(d) shows the effect of dosage on the degradation of MO by using CuO NPs, CDMA@CuO-1 %, CDMA@CuO-2 %, and CDMA@CuO-3 % NC in the aqueous solution was observed at different catalyst dose. Fig. 8(d) shows the %degradtion for the MO at 5 mg, 10 mg, 15 mg, 20 mg and 25 mg with respect to irradiation time. The results obtained exhibited the photocatalytic efficiency of synthesized material towards MO, yielding degradation rate of CuO NPs for 5 mg; 32.37 %, for 10 mg; 57.33 %, for 15 mg; 69.26 %, for 20 mg; 78.31 % and for 25 mg; 65.5 %, for CDMA@CuO-1 %, for 5 mg; 38.54 %, for 10 mg; 68.6 %, for 15 mg; 83.41 %, for 20 mg; 94 % and for 25 mg; 78.31 %, for CDMA@CuO-2 % for 5 mg; 49.83 %, for 10 mg; 76.35 %, 15 mg; 91.15 %, for 20 mg; 96.66 % and for 25 mg; 82.96 % and for CDMA@CuO-3 % for 5 mg; 65.06 %, 10 mg; 87.17 %, 15 mg; 95.33 %, 20 mg; 98.88 % and 25 mg; 89.6 %. It was found that with increases in the dose from 5 mg to 20 mg, more active sites become available for the dye molecules to adsorb onto the surface catalyst. This leads to an increase in the probability of dye molecules coming into conatact with catalyst, thus enhancing the photocatalytic degradation efficiency. The catalyst surface becomes saturated with dye molecules, particularly at higer dose i.e., 25 mg. Once the surface is saturated, additional catalyst dosages may not lead to proportional increase in the degradation efficiency since there are no additional sites available for the adsorption. Therefore, the rate of MO degradation is achieved at 20 mg of catalyst dose in CDMA@Cu-3 NC.

The kinetic efficiency of CDMA@CuO NC and its different configuration towards MO was evaluated by taking 25 mg catalyst with 20 mgL^{-1} concentration of MO at pH 4 for an irradiation time of 90 min. The obtained data was applied to Langmuir-Hinshelwood (L-H) pseudo first order model given by mathematical equation was used-

$$-\ln\frac{C_e}{C_0} = k_1 t$$

$$t_{1/2} = \frac{0.693}{k_1}$$

Fig. 8 (e, f) represents the C_e/C_0 and $-\ln(C_e/C_0)$ vs irradiation time graph respectively, for MO with respect various reaction conditions like (i) MO + light (photolysis) (ii) MO + CDMA@CuO-3 % + no light (adsorption) (iii) CDMA@CuO-3 % + MO + Vis's light (iv) CDMA@CuO-1 % + MO + UV light (v) CDMA@CuO-2 % + MO + UV light (vi) CDMA@CuO-3 % + MO + UV light. In case of photolysis, the rate of MO degradation was negligible (%), indicating that MO does not degrade spontaneously under visible light without a catalyst. During the adsorption process, the material exhibited some extent of adsorption (45 %), attributed to the presence of −OH functionalized biopolymer chains and interlayer of the polymer chains of PMMA. This adsorption process aids in the adhesion of electrically charged MO molecules to the catalyst surface for the subsequent photodegradation. When subjected to UV light irradiation, the CDMA@CuO-1 %, CDMA@CuO-2 %, and CDMA@CuO-3 % demonstrated appreciable MO degradation rate as 84.10 %, 96.50 % and 98.60 % with apparent rate constant value of 0.019, 0.027 and 0.033 min^{-1} and half-life value of 36.47, 25.66 and 21.00 min respectively. It can be seen from Fig. 8 (e, f) and Table 1 that CDMA@CuO-3 % in the presence of visible light exhibited slower rate of degradation towards MO (84.56 %) as compared to UV light (98.60 %).

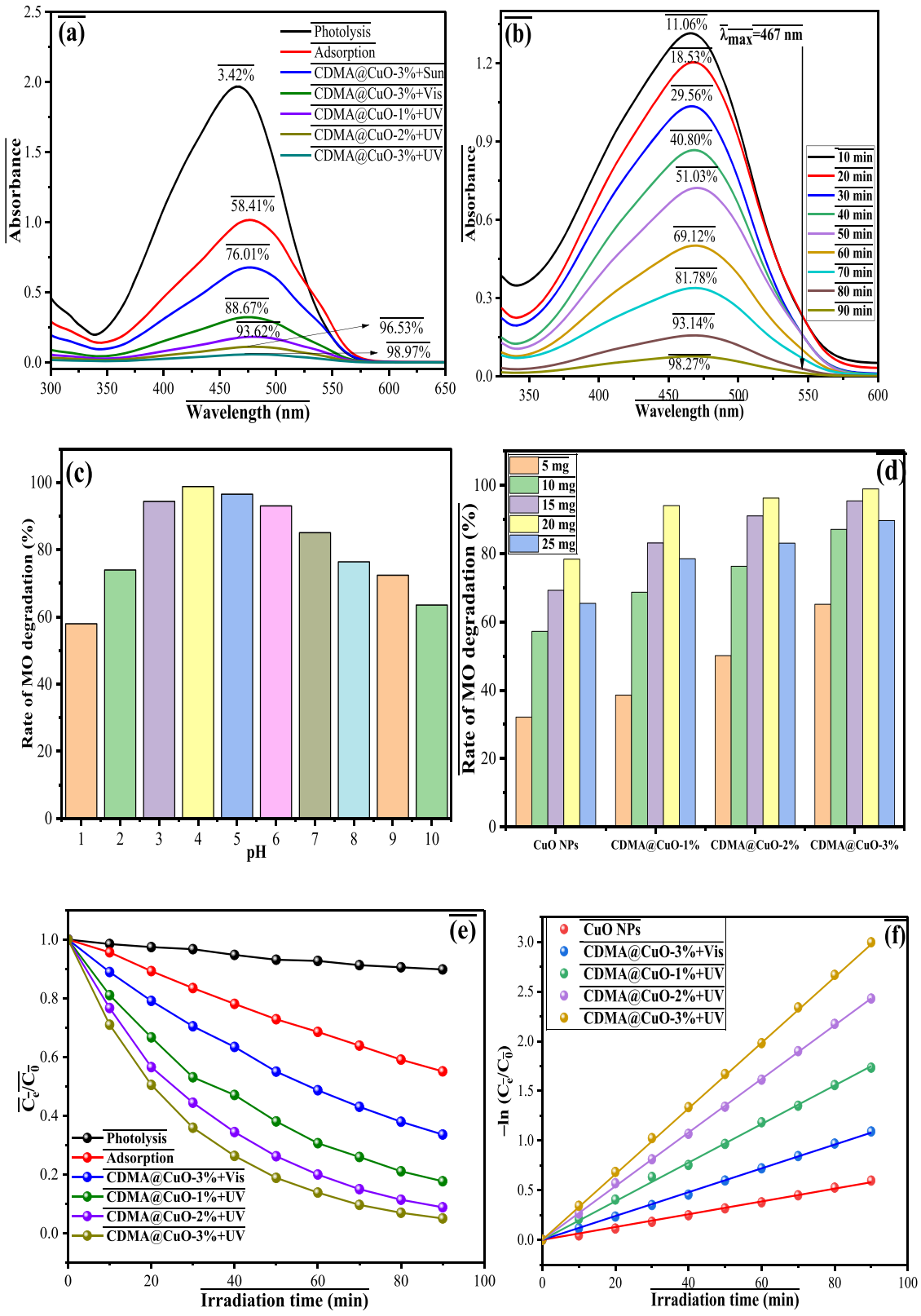

Fig. 8. **(a)** UV spectra of photocatalytic degradation of CDMA@CuO NC and its different concentration at various radiation conditions, **(b)** UV spectra of effect of irradiation time (10–90 min), **(c)** % degradation of effect of pH (1–10), **(d)** % degradation of effect of dose (5–25 mg) of CuO NPs, CDMA@CuO NC and its different concentration **(e, f)** C_e/C_o and -ln (C_e/C_o) concerning time for the photocatalytic degradation of MO dye by CDMA@CuO NC and its different concentration at various radiation conditions.

Table 1
Pseudo-order kinetic parameters for the degradation of MO dye by CDMA@CuO NC.

S.N.	Catalyst	Rate Constant (k_1) (min^{-1})	Half-life $t_{1/2}$ (min)	R^2
1	CDMA@Cu-3 %+Vis	0.012	57.75	0.98
2	CDMA@Cu-1 %+UV	0.019	36.47	0.99
3	CDMA@Cu-2 %+UV	0.027	25.66	0.99
4	CDMA@Cu-3 %+UV	0.033	21.00	0.99

The apparent rate constant was found to be and half-life time will be 0.012 min^{-1} and 57.75 min.

3.4. Scavenger test and degradation mechanism

Species such as e^-, h^+, $^\bullet OH$, and $^\bullet O_2^-$ are recognized as reactive oxidant species (ROS) playing a crucial role in the photodegradation of organic pollutants, transforming them into small non-toxic entities. To elucidate the photodegradation mechanism of ROS, different scavengers were employed like isopropyl alcohol (IPA) as $^\bullet OH$, triphenylphosphine (TPP) as $^\bullet O_2^-$, potassium iodide (SSKI oral solution) as e^- and acrylamide (AA) as h^+ for trapping text. [49,50] The results of these trapping experiments are presented in Fig. 9(a). The trapping experiment involved taking an aliquot of 20 mL of 20 mgL^{-1} of MO dye at pH 4 with a dose of 20 mg for 90 min of CDMA@CuO-3 % NC in the presence of UV light. The outcomes of these experiments shed light on the involvement and impact of specific reactive oxidant species in the photodegradation process [51].

$$\text{(I)}\ \text{CDMA@CuO} - 3\% + h\nu \rightarrow \text{CDMA@CuO} - 3\%(e^-_{CB} + h^+_{VB})$$

$$\text{(II)}\ \text{CDMA@CuO} - 3\%(h^+_{VB}) + H_2O \rightarrow \text{CDMA@CuO} - 3\% + H^+ + {}^\cdot OH$$

$$\text{(III)}\ \text{CDMA@CuO} - 3\%(e^-_{CB}) + O_2 \rightarrow \text{CDMA@CuO} - 3\% + H^+ + {}^\cdot O_2^-$$

$$\text{(IV)}\ {}^\cdot O_2^- + H^+ \rightarrow {}^\bullet HO_2$$

$$\text{(V)}\ \text{CDMA@CuO} - 3\%(e^-_{CB}) + {}^\bullet HO_2 + H^+ \rightarrow H_2O_2$$

$$\text{(VI)}\ \text{CDMA@CuO} - 3\%(e^-_{CB}) + H_2O_2 \rightarrow {}^\cdot OH + OH^-$$

$$\text{(VII)}\ {}^\cdot OH + \text{MO} \rightarrow \text{DegradedMO}$$

When exposed to light radiation, the surface of CDMA@CuO-3 % NC, undergoes the generation of electrons and holes in the conduction and valence bands, respectively. Concurrently, O_2 molecules act as electron (e^-) traps, facilitating the formation of superoxide radicals ($^\bullet O_2^-$). These radicals then react with H^+ ions, giving rise to the formation of $HO_2^\bullet$ radicals, as depicted in the equation (iii, iv). Simultaneously, the holes (h^+) present on the catalyst surface will combine with water, resulting in the formation of $^\bullet OH$ radicals. This process contributes to the photodegradation of MO dye molecules. The $^\bullet OH$ radicals, upon attacking MO dye, facilitate its conversion into non-toxic entities such as CO_2, H_2O, and various byproducts as shown by Scheme 1.

To evaluate further mineralization of MO dye, the total organic carbon (TOC) concentrations in the MO solution were monitored throughout the photodegradation process. As shown in Fig. 9(b), the TOC of the MO solution treated with the CDMA@CuO-3 % NC under UV light irradiation gradually decreased over time. After 90 min, the TOC removal reached 77.36 %, slightly lower than the MB removal rate of 99.52 % based on colour reduction. These findings demonstrate effective mineralization of MO in the CDMA@CuO-3 % NC UV light system, with minimal residual TOC, indicating that CDMA@CuO-3 % NC outperforms previously reported photo-Fenton catalysts in TOC reduction.

3.5. Photocatalytic activity of CDMA@CuO NC and reusability experiement

Fig. 10(a) depicts the UV–Vis curve illustrating the photocatalytic activity of CDMA@CuO-3 % NC and its components in the degradation of MO dye, representing the corresponding percentage degradation in the presence of a UV light source. The photocatalytic experiments were conducted under optimized reaction conditions i.e. MO concentration (20 mgL^{-1}), 90 min at pH 4 with a catalyst amount of 20 mg. The results suggest that the synthesized material demonstrated superior photocatalytic efficiency (98.69 %) compared to its entities of β-CD (39.95 %), PMMA (17.2 %), and CuO NPs (83.95 %). This enhanced photocatalytic activity of CDMA@CuO NC can be attributed to the synergistic properties arising from the absorption of β-CD, PMMA and CuO NPs. The copolymerization on the surface contributes to the increased degradation of MO dye molecules.

In the context of water treatment, the reusability experiment was conducted to assess the stability of the CDMA@CuO-3 % NC material. Following each photocatalytic reaction, the material underwent collection, centrifugation, washing, and drying in the oven before being reused for the subsequent photocatalytic reaction. The reusability experiment adhered to optimized conditions, MO concentration (20 mgL^{-1}) for 90 min at pH 4 with a catalyst dose of 20 mg. This process was repeated for six consecutive cycles, and the results are illustrated in Fig. 10(b). The conclusions drawn from the reusability experiment indicate the photocatalytic efficiency of the synthesized material exhibited high stability over multiple cycles. After 1st cycle, the efficiency was recorded at 98.55 %, followed by 97.14 % in the 2nd cycle,

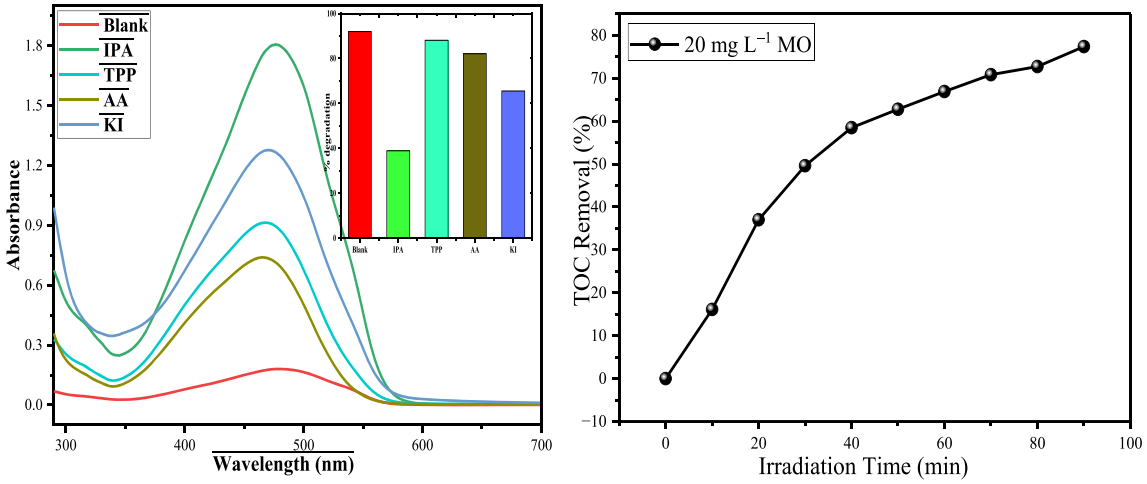

Fig. 9. UV–Vis spectra for the trapping experiment and insert bar show the MO %degradation vs scavenger (b) Total organic carbon (TOC) analysis for MO mineralization by CDMA@CuO-3 % NC.

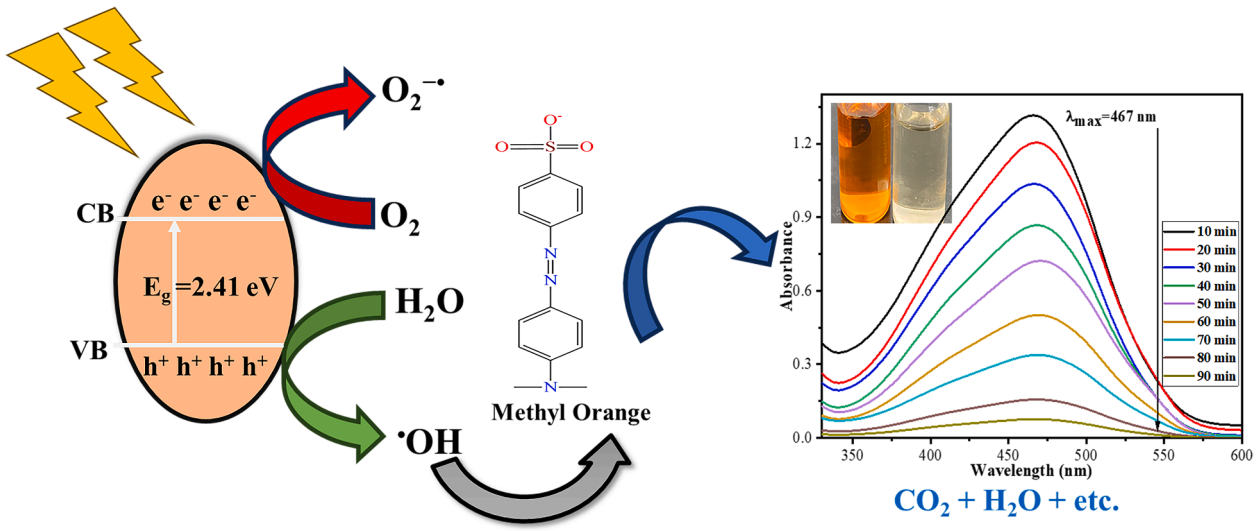

Scheme 1. Mechanism represents the photocatalytic degradation of MO by CDMA@CuO-3 % NC.

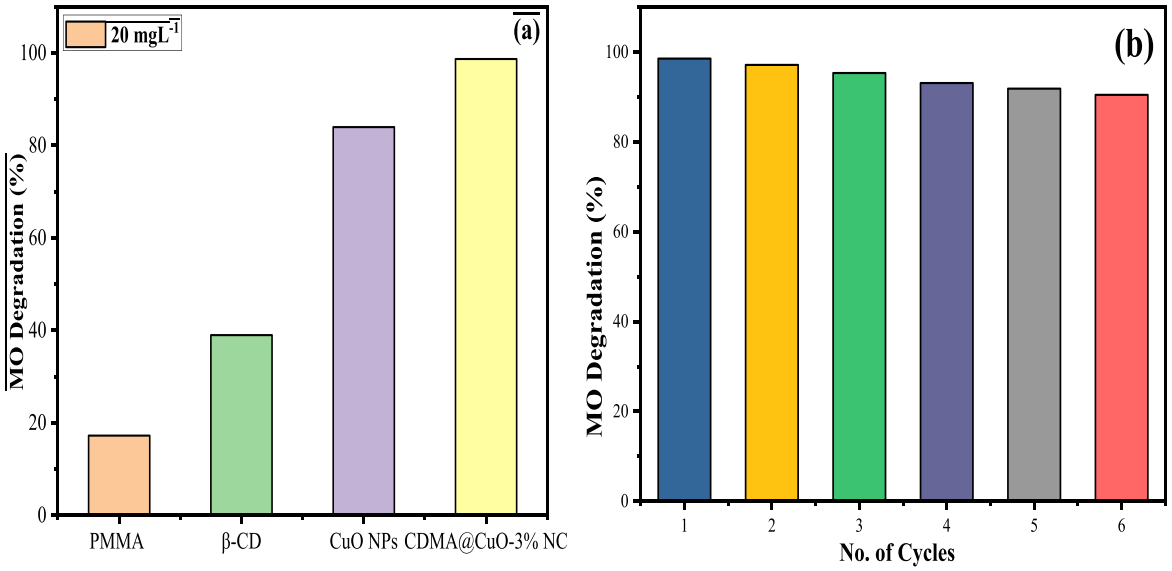

Fig. 10. (a) Photocatalytic degradation of MO by CDMA@CuO-23 % NC and its entities and (b) Reusability plot for the determination of stability of CDMA@CuO-3 % NC.

95.34 % in the 3rd cycle, 93.11 % in the 4th cycle, 91.86 % in the 5th cycle and 90.48 % in the 6th cycle. This suggests that the synthesized material maintains its effectiveness in the photocatalytic degradation of MO dye under optimal conditions and the specified light source.

3.6. Mechanism of MO degradation and indenfication of intermediates formed

The degradation products of methyl orange (MO) dye by CTAG@CuO-3 % NC were identified using LC-MS analysis. Figure S5 shows the total mass spectrograms of MO after 90 min of UV light irradiation. At 0 min (Figure S5 a), a characteristic peak is observed at *m/z* 306, attributed to the positive ion of the MO dye. The mass spectrogram at 90 min (Figure S5 b) shows new *m/z* peaks at 121.1, 156.4, 172.6 and 201.2 corresponding to intermediate products of MO degradation. Identified degradation products include intermediate product formed due to interaction of OH radical with MO molecule at *m/z* 201.2 which further fragments into sulfanilic acid at *m/z* 172.6, which further fragments into benzenesulfonic acid at *m/z* 156.4 after losing an amino group (NH_2). Another product, N,N-dimethylbenzenenamine at *m/z* 121.1 following the loss of an amino group (NH_2). These results are consistent with other studies on MO degradation, though this study achieved complete MO degradation within 90 min significantly faster than previously reported studie. [52,53] The observed results suggest that MO degradation likely involved symmetric cleavage of the azo bond (*–N = N–*), yielding sulfanilic acid and N, N-dimethyl-p-phenylenediamine, followed by further breakdown of these intermediates. As illustrated in Figure S5 (b), the degradation products of MO could potentially mineralize into CO_2 and H_2O under additional conditions, such as $^{\bullet}OH$ radicals and elevated temperature. [54]

3.7. Comparison with literature

The comparison was conducted between synthesized material and material utilizing CuO NPs, considering variointermedaus parameters including irradiation time, light source, pH, concentration, and percentage degradation. Based on the data presented in the Table 2, it is

Table 2
Comparison data of present MO degradation with literature.

Material	Light Source	MO concentration (ppm)	Time	MO dose	%degradation	Reference
ZnO—CuO	UV	100	120	0.3 g	92.18	[55]
p-ZnO-n-CuO	UV	2	15	0.2 mg	96	[56]
CuO/CdS	Vis	30	60	0.75	80	[57]
Cu-doped ZnO	UV	13	120	0.3 g/L	99	[58]
Co-Cu	UV	50	50	0.3 g/L	94	[59]
Degussa P25 TiO_2	UV	10	80	0.5 g/L (MB)	95	[60]
ZnO-TiO_2/clay	UV	75	60	1 g/L (MG)	89.3	[61]
Nano-TiO_2	UV	40	120	0.2 g/L (diazinon)	99.64	[62]
TiO_2/SiO_2	UV	20	120	75 mg	96.05	[63]
rGO-TiO_2	Visible	10	120	0.5 g/L (BPA)	99	[64]
CDMA@CuO NC	UV	20	90	20 mg	99.37	Present study

evident that the current study was more effective and provided additional insights into the photocatalytic degradation of MO dye.

4. Conclusion

The present study elucidates the synthesis of an eco-friendly and cost-effective nanocomposite (NC) through the doping of CuO NPs with PMMA immobilized with β-cyclodextrin. The characteriztion techniques supported the successful synthesis of nanocomposite material. The XPS survey scan of CDMA@CuO-3 % NC, revealing explains the presence of oxygen, carbon, nitrogen, and copper and their chemical states inside the material. The atomic percentage of elements was found to be in CDMA@CuO-1 % was C (64.59 %), O (32.23 %) and Cu (3.18 %) in CDMA@CuO-2 % C (59.01 %), O (34.77 %) and Cu (6.22 %) was and CDMA@CuO-3 % was C (53.78 %), O (37.78 %) and Cu (8.45 %). These results affirm the purity of synthesized material. The material was found to be UV light active and the direct band gap values were calculated as 3.79 eV, 3.18 eV, 2.73 eV and 2.41 eV for pristine CuO NPs, CDMA@CuO-1 %, CDMA@CuO-2 % and CDMA@CuO-3 %. The kinetics studies revealed that the photocatalytic degradation of MO followed pseudo-first-order kinetics, with rate constant (k_1) was found to be 0.012 min^{-1} for CDMA@CuO-3 %-VIS, 0.019 min^{-1} for CDMA@CuO-1 %-UV, 0.027 min^{-1} for CDMA@CuO-2 %-UV and 0.033 min^{-} for CDMA@CuO-3 %-UV with corresponding half-life time ($t_{1/2}$) of 57.75, 36.47, 25.66 and 21.00 min, respectively. Hydroxyl radcals ($^{\bullet}OH$) were found to be primary reactive oxidant species responsible for the degradation of MO in the presence of UV light radiation. According to the reusability experiment, it was observed that after six cycles, the synthesized material exhibited exceptional stability in the degradation of MO dye. In conclusion, this study suggests that the synthesized material holds the potential for the photocatalytic remediations of wastewater for various pollutants.

CRediT authorship contribution statement

Imran Hasan: Writing – review & editing, Visualization, Validation, Supervision, Project administration, Methodology, Funding acquisition, Data curation, Conceptualization. **Akshara Bassi:** Writing – original draft, Software, Resources, Methodology, Investigation, Formal analysis. **Parvathalu Kalakonda:** Writing – review & editing, Validation, Software, Methodology, Data curation, Conceptualization.

Declaration of competing interest

The authors declare that they have no known competing financial interests or personal relationships that could have appeared to influence the work reported in this paper.

Acknowledgement

The authors extend their thanks to Researchers Supporting Project (Ref: RSPD2024R670), King Saud University, Riyadh, Saudi Arabia.

Data availability

The data that support the findings of this study are available from the corresponding author upon reasonable request.

Supplementary materials

Supplementary material associated with this article can be found, in the online version, at doi:10.1016/j.surfin.2024.105456.

Data availability

Data will be made available on request.

References

[1] L. Wang, Z. Li, J. Chen, Y. Huang, H. Zhang, H. Qiu, Enhanced photocatalytic degradation of methyl orange by porous graphene/ZnO nanocomposite, Environ. Pollut. 249 (2019) 801–811, https://doi.org/10.1016/j.envpol.2019.03.071.
[2] R. Shan, L. Lu, J. Gu, Y. Zhang, H. Yuan, Materials Science in semiconductor processing photocatalytic degradation of methyl orange by Ag /TiO 2 / biochar composite catalysts in aqueous solutions, Mater. Sci. Semicond. Process. 114 (April) (2020) 105088, https://doi.org/10.1016/j.mssp.2020.105088.
[3] Jana, M.; Taheruddin, S.; Mitra, M.; Kulsi, C. Visible-light influenced photocatalytic activity of polyaniline -bismuth selenide composites for the degradation of methyl orange, rhodamine b and malachite green dyes applied surface science visible-light in Fl uenced photocatalytic activity of polyanil. 2018, No. November. https://doi.org/10.1016/j.apsusc.2018.11.085.
[4] N. Chankhunthod, P. Junploy, S. Suthirakun, L. Ngamwongwan, C. Phromma, N. Ruchusartsawat, A. Siyasukh, P. Yanu, P. Kijjanapanich, S. Yimklan, A. Rujiwatra, R. Drummond-Brydson, Y. Chimupala, Ecofriendly alkali metal cations diffusion improves fabrication of mixed-phase titania polymorphs on fixed substrate by chemical vapor deposition (CVD) for photocatalytic degradation of azo dye, Environ. Res. 239 (2023) 117347, https://doi.org/10.1016/J.ENVRES.2023.117347.
[5] V.N. Nguyen, D. Trinh, T. Manh, T. Nguyen, Enhanced photocatalytic degradation of methyl orange using ZnO /graphene oxide nanocomposites, Res. Chem. Intermed. 17 (2018), https://doi.org/10.1007/s11164-018-3294-3.
[6] Bhatti, M.A.; Shah, A.A.; Almani, K.F.; Tahira, A. Efficient photo catalysts based on silver doped zno nanorods for the photo degradation of methyl orange. 2019, 45, 23289–23297.
[7] P. Degradation, Nanocomposite of CeVO 4 /BiVO 4 loaded on reduced graphene oxide for the nanocomposite of CeVO 4 / BiVO 4 loaded on reduced graphene oxide for the photocatalytic degradation of methyl orange, J. Clust. Sci. 33 (6) (2022) 2707–2721, https://doi.org/10.1007/s10876-021-02189-z.
[8] V. Quang, T. Khoa, T. Nguyen, A. Khan, Chemosphere photocatalytic degradation of methyl orange dye by Ti 3 C 2 e TiO 2 heterojunction under solar light, Chemosphere 276 (2021) 130154, https://doi.org/10.1016/j.chemosphere.2021.130154.
[9] P.C. Dey, R. Das, Spectrochimica acta part a: molecular and biomolecular spectroscopy enhanced photocatalytic degradation of methyl orange dye on interaction with synthesized ligand free CdS nanocrystals under visible light illumination, Spectrochim. Acta Part A Mol. Biomol. Spectrosc. 231 (2020) 118122, https://doi.org/10.1016/j.saa.2020.118122.
[10] S. Limsakul, T. Mahatnirunkul, C. Phromma, T. Chomtong, N. Cholnakasem, S. Yimklan, P. Ruankham, A. Siyasukh, Y. Chimupala, Novel Physical Sunscreen from One-dimensional TiO2 nanowire: synthesis, characterization and the effects of morphologies and particle size for use as a physical sunscreen, Nano-Struct.

Nano-Objects 35 (2023) 101027, https://doi.org/10.1016/J.NANOSO.2023.101027.
[11] I. Ali, A. Arsh, X.Y. Mbianda, A. Burakov, E. Galunin, I. Burakova, E. Mkrtchyan, A. Tkachev, V. Grachev, Graphene based adsorbents for remediation of noxious pollutants from wastewater, Environ Int 127 (January) (2019) 160–180, https://doi.org/10.1016/j.envint.2019.03.029.
[12] J. Bhadra, H. Parangusan, A. Popelka, M. Lehocky, P. Humpolicek, N. Al-thani, Journal of environmental chemical engineering electrospun polystyrene /PANI-Ag Fi Bers for organic dye removal and antibacterial application, J. Environ. Chem. Eng. 8 (3) (2020) 103746, https://doi.org/10.1016/j.jece.2020.103746.
[13] T.V.L. Thejaswini, D. Prabhakaran, M.A. Maheswari, Ultrasound assisted synthesis of nano-rod embedded petal designed α-Bi2O3-ZnO nanoparticles and their ultra-responsive visible light induced photocatalytic properties, J. Photochem. Photobiol. A Chem. 335 (2017) 217–229, https://doi.org/10.1016/j.jphotochem.2016.12.001.
[14] Varjani, S.; Rakholiya, P.; Ng, H.Y.; You, S.; Teixeira, J.A. Bioresource technology microbial degradation of dyes : an overview. 2020, 314 (June). https://doi.org/10.1016/j.biortech.2020.123728.
[15] Li, J.; Lu, T.; Zhao, Z.; Xu, R.; Li, Y.; Huang, Y.; Yang, C.; Zhang, S. Preparation of heterostructured ternary Cd /CdS / BiOCl photocatalysts for enhanced visible-light photocatalytic degradation of organic pollutants in wastewater. 2020, 121 (July). https://doi.org/10.1016/j.inoche.2020.108236.
[16] A. Somdee, S. Wannapop, Enhanced photocatalytic behavior of ZnO nanorods decorated with a Au, ZnWO4, and Au/ZnWO4 composite: synthesis and characterization, Colloid Interface Sci. Commun. 47 (2022) 100591, https://doi.org/10.1016/J.COLCOM.2022.100591.
[17] C. Byrne, G. Subramanian, S.C. Pillai, Journal of environmental chemical engineering recent advances in photocatalysis for environmental applications, J. Environ. Chem. Eng. 6 (3) (2018) 3531–3555, https://doi.org/10.1016/j.jece.2017.07.080.
[18] M.S. Nasrollahzadeh, M. Hadavifar, S.S. Ghasemi, M. Arab Chamjangali, Synthesis of ZnO nanostructure using activated carbon for photocatalytic degradation of methyl orange from aqueous solutions, Appl. Water Sci. 8 (4) (2018), https://doi.org/10.1007/s13201-018-0750-6.
[19] P.V. Prasath, R. Parthiban, F. Mohammad, W.C.Of. Oh, Opt. - Int. J. Light Electron Opt. (2020) 164428, https://doi.org/10.1016/j.ijleo.2020.164428.
[20] Y. Lv, J. Liu, Z. Zhang, W. Zhang, A. Wang, F. Tian, Green synthesis of CuO nanoparticles-loaded ZnO nanowires arrays with enhanced photocatalytic activity, Mater. Chem. Phys. 267 (May) (2021) 124703, https://doi.org/10.1016/j.matchemphys.2021.124703.
[21] S. Sharma, K. Kumar, N. Thakur, S. Chauhan, Journal of environmental chemical engineering eco-friendly ocimum tenuiflorum green route synthesis of CuO nanoparticles : characterizations on photocatalytic and antibacterial activities, J. Environ. Chem. Eng. 9 (4) (2021) 105395, https://doi.org/10.1016/j.jece.2021.105395.
[22] M. Rakibul, S. Shahriyar, A. Kabir, F.U. Farhad, Colloids and surfaces A : physicochemical and engineering aspects synthesis, characterization and visible light-responsive photocatalysis properties of Ce doped CuO nanoparticles : a combined experimental and DFT + U study, Colloids Surfaces A Physicochem. Eng. Asp. 617 (February) (2021) 126386, https://doi.org/10.1016/j.colsurfa.2021.126386.
[23] S.J. Singh, P. Chinnamuthu, Colloids and Surfaces a : physicochemical and engineering aspects highly efficient natural-sunlight-driven photodegradation of organic dyes with combustion derived Ce-doped CuO nanoparticles, Colloids Surfaces A Physicochem. Eng. Asp. 625 (May) (2021) 126864, https://doi.org/10.1016/j.colsurfa.2021.126864.
[24] S. Wannapop, A. Somdee, Highly orientated one-dimensional Cu2O/TiO2 heterostructure thin film for photoelectrochemical photoanode and photocatalytic degradation applications, Thin. Solid. Films 747 (2022) 139144, https://doi.org/10.1016/J.TSF.2022.139144.
[25] D. Chaves, M.I. Yoshida, J. Carlos, C. Freitas De, D.F. Cipriano, β-Cyclodextrin inclusion complexes with essential oils: obtention, characterization, antimicrobial activity and potential application for food preservative sachets, Food Res. Int. (2019), https://doi.org/10.1016/j.foodres.2019.01.016. #pagerange#.
[26] Q. Huang, K. Chai, L. Zhou, H. Ji, A Phenyl-Rich β- cyclodextrin porous crosslinked polymer for efficient removal of aromatic pollutants : insight into adsorption performance and mechanism, Chem. Eng. J. (2020) 124020, https://doi.org/10.1016/j.cej.2020.124020.
[27] M.R. Bindhu, P. Saranya, M. Sheeba, C. Vijilvani, T.S. Rejiniemon, A.M. Al-mohaimeed, M. Ragab, M. Soliman, Functionalization of gold nanoparticles by β -cyclodextrin as a probe for the detection of heavy metals in water and photocatalytic degradation of textile dye, Environ. Res. 201 (May) (2021) 111628, https://doi.org/10.1016/j.envres.2021.111628.
[28] A. Dehghani, G. Bahlakeh, B. Ramezanzadeh, Designing a Novel Targeted-Release Nano-Container Based On the Silanized Graphene Oxide Decorated With Cerium Acetylacetonate, Elsevier B.V., 2020, https://doi.org/10.1016/j.cej.2020.125860.
[29] Musa, M.S.; Rusli, A.; Ariffin, A.; Shafiq, M.D. Polymerization and applications of Poly(methyl methacrylate) – graphene oxide nanocomposites: a review. 2022. https://doi.org/10.1021/acsomega.2c04483.
[30] O. Ounas, A. Anouar, E. Foulani, B. Lekhlif, J. Jamal-eddine, Materials today : proceedings immobilization of TiO 2 into a poly methyl methacrylate (PMMA) as hybrid film for photocatalytic degradation of methylene blue, in: Mater. TODAY Proc., 2019, https://doi.org/10.1016/j.matpr.2019.08.068. No. xxxx.
[31] A. Gupta, N. Khosla, V.G. Amit, S.K. Annapurna, Trimetallic composite nanofibers for antibacterial and photocatalytic dye degradation of mixed dye water, Appl. Nanosci. 2 (0123456789) (2020), https://doi.org/10.1007/s13204-020-01540-6.
[32] Taha, J.H.; Abbas, N.K.; Al-attraqchi, A.A.F. Green synthesis and evaluation of copper oxide nanoparticles using fig leaves green synthesis and evaluation of copper oxide nanoparticles using fig leaves and their antifungal and antibacterial activities. 2020, No. September. https://doi.org/10.25258/ijddt.10.3.13.
[33] A. Karthika, D.R. Rosaline, S.S.R. Inbanathan, A. Suganthi, M. Rajarajan, Journal of physics and chemistry of solids fabrication of cupric oxide decorated β -cyclodextrin nanocomposite solubilized Na Fi on as a high performance electrochemical sensor for L - tyrosine detection, J. Phys. Chem. Solids 136 (July 2019) (2020) 109145, https://doi.org/10.1016/j.jpcs.2019.109145.
[34] A.M.El Sayed, Preparation and characterization of CuO /Co 3 O 4 / Poly (Methyl Methacrylate) nanocomposites for optical and dielectric applications, J Mater Sci Mater Electron. (2021), https://doi.org/10.1007/s10854-021-05949-9.
[35] J. Sarkar, N. Chakraborty, A. Chatterjee, A. Bhattacharjee, Green synthesized copper oxide nanoparticles ameliorate defence and antioxidant enzymes in lens culinaris, Nanomaterials 10 (2) (2020) 312. https://doi.org/10.3390/nano10020312.
[36] Chemistry, A.; Africa, S.; Island, W.; State, Y.B. Ournal Of. 2018, 30 (4), 859–867.
[37] I. Hasan, F.A. Alharthi, Journal of photochemistry & photobiology, A : chemistry caffeine-alginate immobilized CeTiO 4 bionanocomposite for efficient photocatalytic degradation of methylene blue, J. Photochem. Photobiol. A Chem. 433 (March) (2022) 114126, https://doi.org/10.1016/j.jphotochem.2022.114126.
[38] H. C. Finely dispersed CuO on nitrogen-doped carbon hollow nanospheres for selective oxidation of Sp 3. 2021. https://doi.org/10.1039/d1nj02406j.
[39] Y. Wang, X. Dong, L. Zhao, Y. Xue, X. Zhao, Q. Li, Y. Xia, Facile and green fabrication of carrageenan-silver nanoparticles for colorimetric determination of Cu2+ and S2−, Nanomaterials 10 (1) (2020) https://doi.org/10.3390/nano10010083.
[40] Online, V.A.; Chen, S.; Karuppiah, C.; Lou, B. RSC advances. 2016. https://doi.org/10.1039/C6RA10130E.
[41] RGO @ CuO Nanocomposites from A renewable copper mineral precursor: a green approach for decarboxylative C (Sp 3) -H Activation of proline amino acid to afford value-added synthons. 2018. https://doi.org/10.1021/acssuschemeng.8b01376.
[42] Aroussi, S.; Dahamni, M.A.; Ghamnia, M.; Tonneau, D.; Fauquet, C. Characterization of Some Physical and Photocatalytic Properties of CuO Nanofilms Synthesized by a Gentle Chemical Technique. 2022.
[43] A.K. Nikolaidis, D.S. Achilias, Thermal degradation kinetics and viscoelastic behavior of Poly(Methyl Methacrylate)/organomodified montmorillonite nanocomposites prepared via in situ bulk radical polymerization, Polymers (Basel) 10 (5) (2018), https://doi.org/10.3390/polym10050491.
[44] H.M. Alghamdi, A. Rajeh, Study of the photoluminescence, optical, thermal, and electrical parameters of the Cs/PVP Blend/Zinc oxide nanorods films for energy storage devices, Polym. Test. 124 (2023) 108093, https://doi.org/10.1016/J.POLYMERTESTING.2023.108093.
[45] G. Magesh, G. Bhoopathi, N. Nithya, A.P. Arun, E. Ranjith Kumar, Effect of biopolymer blend matrix on structural, optical and biological properties of chitosan–agar blend ZnO nanocomposites, J. Inorg. Organomet. Polym. Mater. 28 (4) (2018) 1528–1539, https://doi.org/10.1007/S10904-018-0848-1/METRICS.
[46] H.L.S. Santos, P.G. Corradini, M.A.S. Andrade, L.H. Mascaro, CuO/NiOx thin film–based photocathodes for photoelectrochemical water splitting, J. Solid State Electrochem. 24 (8) (2020) 1899–1908, https://doi.org/10.1007/S10008-020-04513-5/METRICS.
[47] D.P. Sahoo, S. Patnaik, D. Rath, B. Nanda, K. Parida, Cu@CuO promoted G-C3N4/MCM-41: an efficient photocatalyst with tunable valence transition for visible light induced hydrogen generation, RSC Adv. 6 (113) (2016) 112602–112613, https://doi.org/10.1039/C6RA24358D.
[48] H. Cui, W. Wang, J. Sha, S. Li, J. Zhuo, M. Hu, Vesicular mesoporous copper oxide as anode for high lithium storage, J. Mater. Sci. Mater. Med. 34 (11) (2023) 1–11, https://doi.org/10.1007/S10854-023-10356-3/METRICS.
[49] A.F. Zedan, A.T. Mohamed, M.S. El-Shall, S.Y. Alqaradawi, A.S. Aljaber, Tailoring the reducibility and catalytic activity of CuO nanoparticles for low temperature CO oxidation, RSC Adv. 8 (35) (2018) 19499–19511, https://doi.org/10.1039/C8RA03623C.
[50] Karbasi, M., Karimzadeh, F., Raeissi, K., Rtimi, S., Kiwi, J., Giannakis, S., & Pulgarin, C. (2020). Insights into the Photocatalytic Bacterial Inactivation by Flower-Like Bi2WO6 under Solar or Visible Light, Through in Situ Monitoring and Determination of Reactive Oxygen Species (ROS). Water 2020, 12, 1099, 12(4), 1099. https://doi.org/10.3390/W12041099.
[51] A. Bassi, I. Hasan, K. Qanungo, B.H. Koo, R.A. Khan, Visible light assisted mineralization of malachite green dye by green synthesized xanthan gum/agar@ZnO bionanocomposite, J. Molec. Struct. 1256 (2022) 132518. https://doi.org/10.1016/J.MOLSTRUC.2022.132518.
[52] S. Xie, P. Huang, J.J. Kruzic, X. Zeng, H. Qian, A highly efficient degradation mechanism of methyl orange using fe-based metallic glass powders, Sci. Rep. 6 (1) (2016) 1–10, https://doi.org/10.1038/srep21947. *2016 6:1*.
[53] S. Kumari, A. Kumari, A. Kandwal, J. Ahmed, S.M. Alshehri, R. Jasrotia, R. Sharma, Activation of nanoparticles of nickel ferrite by divalent metal ions Co-doping for the methyl orange dye's photocatalytic degradation: a kinetic and adsorption isotherm study, Clean Technol. Environ. Policy (2023) 1–18, https://doi.org/10.1007/S10098-023-02667-0/METRICS.
[54] B. Lai, Q. Ji, Y. Yuan, D. Yuan, Y. Zhou, J. Wang, Degradation of ultrahigh concentration pollutant by Fe/Cu bimetallic system at high operating temperature, Korean J. Chem. Eng. 33 (1) (2015) 207–215, https://doi.org/10.1007/S11814-015-0135-6. *2016 33:1*.
[55] M. Gerawork, Photodegradation of methyl orange dye by using zinc oxide – copper oxide nanocomposite, Optik (Stuttg) 216 (April) (2020), https://doi.org/10.1016/j.ijleo.2020.164864.

[56] N. Basavegowda, P. Somu, A.M. Shabbirahmed, L.A. Gomez, J.J. Thathapudi, Bimetallic P-ZnO/n-CuO nanocomposite synthesized using aegle marmelos leaf extract exhibits excellent visible-light-driven photocatalytic removal of 4-nitroaniline and methyl orange, Photochem. Photobiol. Sci. 21 (8) (2022) 1357–1370, https://doi.org/10.1007/s43630-022-00224-0.
[57] S.S. Hossain, M. Tarek, T.D. Munusamy, K.M. Rezaul Karim, S.M. Roopan, S. M. Sarkar, C.K. Cheng, M.M. Rahman Khan, Facile synthesis of CuO/CdS heterostructure photocatalyst for the effective degradation of dye under visible light, Environ. Res. 188 (2020) 109803, https://doi.org/10.1016/j.envres.2020.109803.
[58] Atia, M.N.; communications, M. T. SC. 2018.
[59] B. Zhang, Y. Yan, S. Chen, X. Xu, C. Wu, Preparation of a novel copper–cobalt composite catalyst and study on performance degradation of methyl orange, Processes 11 (11) (2023), https://doi.org/10.3390/pr11113238.
[60] S.M. Tichapondwa, J.P. Newman, O. Kubheka, Effect of TiO2 phase on the photocatalytic degradation of methylene blue dye, Phys. Chem. Earth (2020) 102900, https://doi.org/10.1016/j.pce.2020.102900.
[61] H. Bel, M. Ben, M. Elena, P. Da, Journal of photochemistry and photobiology a : chemistry photocatalytic degradation of methyl green dye in aqueous solution over natural clay-supported ZnO – TiO 2 catalysts, J. Photochem. *Photobiol. A Chem.* 315 (2016) 25–33, https://doi.org/10.1016/j.jphotochem.2015.09.008.
[62] Taylor, P.; Kalantary, R.R.; Shahamat, Y.D.; Farzadkia, M.; Esrafili, A. Desalination and water treatment photocatalytic degradation and mineralization of diazinon in aqueous solution using nano-TiO 2 (Degussa, P25): kinetic and statistical analysis. 2014, No. July, 37–41. https://doi.org/10.1080/19443994.2014.928795.
[63] Eddy, D.R.; Ishmah, S.N.; Permana, M.D.; Firdaus, M.L.; Rahayu, I.; El-badry, Y.A.; Hussein, E.E.; El-bahy, Z.M. Applied sciences photocatalytic phenol degradation by silica-modified titanium dioxide. 2021.
[64] Yu, F.; Bai, X.; Yang, C.; Xu, L. Reduced graphene oxide – P25 nanocomposites As. 1831.